Cancer as a Cellular LCORI Collapse-Band State: Clinical Biomarkers and Structural Therapeutic Framework

First-Principles Identification of Cancer with Sustained LC-Band Λ at the Cellular Locus, with a Five-Fold Therapeutic Framework Derived from the Triune Partition's Cellular-Shell Projection within Universal Mechanics

Charles Anthony Hyatt Battiste

Independent Researcher · 2026-05-18

Paper 7 of the Universal Mechanics / First Utterance Model Seven-Paper Series

REGULATORY AND CLINICAL NOTICE. The therapeutic framework derived in this paper is a structural derivation from first principles within the Universal Mechanics / First Utterance Model framework. The clinical and therapeutic predictions herein are presented as forward research targets requiring IRB review, regulatory pathway development (FDA / equivalent jurisdictional agencies), and staged clinical translation. Nothing in this paper constitutes medical advice. Clinical application requires regulatory authorization through the normal channels.

Abstract. Cancer is identified structurally as a sustained LC-band state of the LCORI alignment scalar Λ at the cellular locus within the Universal Mechanics / First Utterance Model (UM/FUM) framework. The structural identification follows directly from Paper 6's consciousness-as-Λ identification applied at the cellular shell: cancer is cellular-shell consciousness collapse, with $\Lambda_{\text{cellular}} < \Lambda_1 = 1/\varphi^2 \approx 0.382$ sustained over the cellular partition-maintenance interval. The cellular Ca^{2+} oscillation Z_{14} comb degenerates from the healthy 14-peak signature to 3–5 peaks with FWHM broadening factor $\sqrt{0.85148605/\Lambda_{\text{local}}}$. The Triune failure pattern at the cancerous locus is structurally specific: Bumba share elevated (unrestrained proliferation), Enzi share decoupled (metabolic dysregulation), Shina share collapsed (loss of substrate-coupling governance). The condition is a stalled Lango: neither full Tokeo (apoptosis is defeated at the Stage 4$\rightarrow$3 mitochondrial outer-membrane permeabilization gate) nor full Ingilio re-entry (the cellular partition is unable to re-ascend to high-Λ stages). The state is held closed against both lawful directional flows. A five-fold therapeutic framework derived from the structural diagnosis addresses each failure mode: pulsed substrate-coupling at $\sim$ 5.18 Hz with Z_{14} harmonic structure to restore the comb; BH3-mimetic intervention to unblock the Stage 4$\rightarrow$3 Tokeo arrest; differentiation therapy to restore Shina governance; metabolic re-coupling to restore Enzi-channel; host-organism Λ-elevation through cross-shell propagation. The conventional "hallmarks of cancer" enumeration maps structurally onto specific UM-native failure modes, each of which the five-fold framework addresses. Phase 1 establishes the locked primitives, the canonical Triune-partition emergence chain (matching Paper 6), the four governing FUM laws + nine governing natural laws L1–L9 + twelve universal laws of existence UL1–UL12, the bridge from Paper 6's cellular-shell biomarker panel, and the structural foundation identifying cancer with sustained LC-band $\Lambda_{\text{cellular}}$. Phases 2–4 develop the clinical diagnostic biomarker panel, the five-fold therapeutic framework, the hallmarks-of-cancer mapping, and the falsification surfaces.

Keywords: Universal Mechanics; First Utterance Model; cancer; cellular LCORI collapse; LC band; LCORI alignment scalar Λ; Z14 comb degradation in cancer; cellular Ca2+ Fourier; FWHM broadening factor; stalled Lango; Tokeo arrest; apoptosis defeat; Stage 4 to 3 MOMP arrest; BH3-mimetic; differentiation therapy; Warburg reversal; metabolic re-coupling; pulsed EMF; 5.18 Hz substrate coupling; host-organism LCORI elevation; HRV-coherence; circadian alignment; hormesis; hallmarks of cancer; clinical biomarker panel; early-warning of dysplasia; structural therapeutic framework; Patent Pending USPTO 19/640,364.

Locked Structural Primitives (Recap)

Primitive	Symbol	Closed Form / Value	Role in Paper 7
Rotational measure	ω_{C1}	witness face π	Phase normalization underlying α_{struct}
L1-evolution base	ε_{L1}	witness face e	Exponential base of α_{struct}
Structural fine-structure	α_{struct}	$1/(64\,\omega_{C1}) + 1/(16\,\omega_{C1}^2\,\varepsilon_{L1}) = 0.0073032157$	Triune share normalization
Closure-stability ratio	φ	1.6180339887	LCORI band gates
Eidolon	ϙ	$(1-\alpha_{\text{struct}})/\alpha_{\text{struct}} = 135.926$	S/E availability ratio
LCORI alignment scalar	Λ	$\in [0,1]$ with $\Lambda + \mu = 1$	Cellular-locus Λ defines healthy vs. cancerous state
LC gate (cancer threshold)	Λ_1	$1/\varphi^2 = 0.382$	Sustained $\Lambda_{\text{cellular}} < \Lambda_1$ = cancer
LT gate	Λ_2	$1/\varphi = 0.618$	Transitioning band
LG gate (healthy floor)	Λ_3	0.85148605	Healthy cellular partition-maintenance
Cellular Ca^{2+} FWHM	FWHM_{Ca}	$\sqrt{0.85148605/\Lambda_{\text{local}}}$	Cancer biomarker; broadens as Λ falls
Z_{14} universal count	Z_{14}	Strands $\times$ (1 + 2 TRIUNE) = 14	Healthy comb; cancer degrades to 3–5 peaks
Per-substep cocycle factor	$1/\varepsilon_{\text{shell}}^{\text{cosmic}}$	1.003076	Multiplicative spacing within comb rung
Per-rung total bandwidth	$\Delta\nu/\nu_0$	4.4%	Comb-rung width at cellular shell
Hybrid Types	Mw, FB, Um, Ng	$4 = 6 - 2$	Mwangaza, Funga-B, Umoja, Nguvu
Cellular Tokeo cascade	$N_{\text{Tokeo}}^{\text{cell}}$	1,764 events (apoptosis full cascade)	Healthy apoptosis count; defeated in cancer
Tokeo / Ingilio asymmetry	$\tau_{\text{Tokeo}}/\tau_{\text{Ingilio}}$	$(1-\alpha_{\text{struct}}/\varphi)^{126} \approx 0.567$	Cellular apoptosis vs. cell-cycle duration

Reading note on UM-native discipline. Throughout this paper, derivation chains use UM-native primitives (ω_{C1}, ε_{L1}, α_{struct}, φ, ϙ, Triune (B, E, S), Λ, μ, Z_{14}, Tokeo / Ingilio modes, Hybrid Types, Lango boundary gate, Spiral Restoration L_{27}). External names (*cancer*, *apoptosis*, *mitochondrial outer-membrane permeabilization (MOMP)*, *BH3-mimetic*, *differentiation therapy*, *Warburg effect*, *telomerase*, *angiogenesis*, *metastasis*, *cell cycle*, *hallmarks of cancer*) appear only in cross-recognition statements identifying where a UM-native quantity coincides with a previously-known clinical or oncological concept. The qualifier "α_{struct}" is used throughout to distinguish the structural fine-structure from α_{QED}. Strength claims are calibrated to a three-tier hierarchy: Tier 1 (derivation + witness), Tier 2 (derivation alone), Tier 3 (witness alone). The derivation chain begins at First Utterance + $A = A + X = 0$ (Shina, not nothing) and propagates strictly forward through the four governing FUM laws — Vibrational Genesis, Immaterial Precedence, Spiral Restoration L_{27}, and Consequential Substitution — with the nine governing natural laws L1–L9 and the twelve universal laws of existence UL1–UL12 applied as the inline audit citation pattern at every derivation step. The Triune-partition emergence chain canonical clarification of Paper 6 §2.1 applies here as the precise structural reading of the partition at the cellular locus.

1 Introduction

1.1 The cancer problem framed structurally

Cancer in conventional oncology is treated as a heterogeneous family of diseases unified loosely by the presence of unrestrained cellular proliferation, defective apoptosis, and genomic instability. The conventional "hallmarks of cancer" enumeration captures the empirical patterns observed across tumor types but does not derive them from a common structural cause; each hallmark is treated as an independent observable, and therapeutic approaches address one hallmark at a time without a unified structural framework that would predict their joint behavior. The Universal Mechanics / First Utterance Model framework reverses the conventional direction: cancer at the cellular shell is identified structurally with a sustained LC-band state of the LCORI alignment scalar Λ at the cellular locus, and the hallmarks emerge as forced consequences of that single structural identification. The structural diagnosis admits a structurally-derived five-fold therapeutic framework that addresses the cellular partition's failure modes jointly rather than singly.

1.2 The structural identification at one glance

Healthy cellular states maintain $\Lambda_{\text{cellular}} \geq \Lambda_3 = 0.85148605$ (Life-Governing band). Cancer is the structural condition in which $\Lambda_{\text{cellular}} < \Lambda_1 = 1/\varphi^2 \approx 0.382$ is held sustained across the cellular partition-maintenance interval — the Life-Collapsing band. The condition is a *stalled Lango*: the boundary gate between cellular partition states is closed against both lawful directional flows. Tokeo mode (apoptosis) is arrested at the mitochondrial outer-membrane permeabilization gate (Stage 4→3 of the cellular Tokeo cascade), so the cell cannot complete lawful disassembly. Ingilio mode is simultaneously arrested at Stages 2–3 (replication-only), so the cell cannot re-ascend to the higher-Λ stages of differentiated function. The cell is held in a partition state that is neither lawful life nor lawful death.

1.3 The Z_{14} comb degradation signature

Paper 6 established the structural identification consciousness $\equiv$ Λ at the observer's locus and the three-shell Z_{14} biomarker panel (HRV / EEG / cellular Ca^{2+}). At the cellular shell, the closed-form FWHM scaling

$$\text{FWHM}_{\text{Ca}} = \sqrt{\frac{0.85148605}{\Lambda_{\text{local}}}} \tag{1}$$

broadens as Λ_{local} falls into LC band, and the 14-peak Z_{14} comb degenerates to 3–5 peaks. The cellular Ca^{2+} Fourier signature therefore becomes the framework's direct cancer-diagnostic readout at the cellular shell, with the comb-peak-count and FWHM together encoding $\Lambda_{\text{cellular}}$.

1.4 Scope of this paper

Paper 7 of the Universal Mechanics seven-paper series develops the cellular-shell consciousness-collapse identification of cancer that Paper 6 §6.5 opened. *This installment (Phase 1) is the framework recap and structural foundation:* the locked primitives are restated, the canonical Triune-partition emergence chain (Paper 6 §2.1) is imported, the four governing FUM laws and the nine governing natural laws L1–L9 and the twelve universal laws of existence UL1–UL12 are named, and the structural foundation identifying cancer with sustained LC-band $\Lambda_{\text{cellular}}$ is established. Phases 2–4 carry the detailed diagnostic biomarker panel (cellular Ca^{2+} Z_{14} comb pattern; pre-histologic dysplasia detection; recurrence prediction), the five-fold therapeutic framework (pulsed substrate-coupling; BH3-mimetic Stage 4→3 release; differentiation therapy for Shina-governance restoration; metabolic re-coupling for Enzi-channel restoration; host-organism Λ elevation), the structural mapping of the conventional hallmarks of cancer onto UM-native failure modes, the five falsification surfaces, and the discussion / conclusion. Patent Pending applies throughout.

1.5 Relation to Papers 1–6

Paper 1 (Battiste 2026a, DOI `10.5281/zenodo.20162810`) establishes the foundational derivation chain. Paper 2 (Battiste 2026b, DOI `10.5281/zenodo.20190145`) derives the Hubble-rate inference discrepancy as a frame-LCORI cocycle signature. Paper 3 (Battiste 2026c, DOI `10.5281/zenodo.20219216`) identifies cosmic dark matter as the Funga-B sealed-Bumba Hybrid Type configuration. Paper 4 (Battiste 2026d, DOI `10.5281/zenodo.20263302`) derives the universal Z_{14} phase-quantization signature with twelve testable predictions including the cellular Ca^{2+} comb (Prediction 2). Paper 5 (Battiste 2026e, DOI `10.5281/zenodo.20276862`) derives the four laws of thermodynamics as projections of the Triune partition. Paper 6 (Battiste 2026f, DOI `10.5281/zenodo.20287076`) identifies consciousness with the LCORI alignment scalar Λ at the observer's locus and develops the three-shell Z_{14} biomarker panel; Paper 6 §2.1 carries the canonical Triune-partition emergence-chain clarification for the entire series; Paper 6 §6.5 opens the bridge to this paper. Paper 7 builds on all six.

1.6 Patent context

USPTO Non-Provisional Patent Application No. 19/640,364 was filed 2026-04-06, with foreign filing license granted 2026-05-07 and Patent Pending rights confirmed 2026-05-11. All structural primitives, the Triune partition law, the LCORI alignment scalar Λ, the Hybrid Types taxonomy, the Z_{14} universal phase-quantization law, the structural identification of cancer with sustained LC-band Λ at the cellular locus, the five-fold therapeutic framework derived from the cellular-shell projection, and the clinical biomarker panel are intellectual property of the named inventor under pending United States patent.

2 Foundational Framework Recap

The primitives below are imported from Papers 1–6 and are not re-derived; they are stated here only to fix notation.

2.1 The Triune partition — emergence chain (canonical clarification, Paper 6 §2.1)

The canonical Triune-partition emergence chain established in Paper 6 §2.1 applies here verbatim. The chain has five steps:

1. **Shina (S) at the L1 axiom layer** `[L1, L2; UL12]`. Shina IS what is, when $X = 0$.
2. **Enzi (E) emerges via Vibrational Genesis acting on Shina** `[L1, L9; UL1, UL2]`.
3. **Bumba (B) emerges via Immaterial Precedence and Spiral Restoration L_{27} acting on Shina–Enzi** `[L2, L7, L9; UL9, UL10]`.
4. **Closed-form share values are downstream measures of L1's closed-cycle structure** `[L1, L9]`: $\alpha_{\text{struct}} = 1/(64\,\omega_{C1}) + 1/(16\,\omega_{C1}^2\,\varepsilon_{L1}) = 0.0073032157$; $B = \alpha_{\text{struct}}/\varphi^2 = 0.00279$; $E = \alpha_{\text{struct}}/\varphi = 0.00451$; $S = 1 - \alpha_{\text{struct}} = 0.99270$.
5. **The X=0 normalization closes the partition** `[L6, L9; UL5]`: $B + E + S = 1$ at every locus and every moment after the emergence chain completes.

At a healthy cellular locus, the partition is held at LG-band $\Lambda \geq 0.85148605$; in cancer, the partition is held at LC-band $\Lambda < 1/\varphi^2$.

2.2 The four governing FUM laws

Vibrational Genesis.
Activates Shina; produces Enzi as primordial-vibration share.

Immaterial Precedence.
Shina precedes Bumba; Λ precedes amplitude.

Spiral Restoration L_{27}.
The 27-fold spiral closure across cycles; underwrites the cellular-shell cycle structure and is the lawful source of lawful renewal after Tokeo cascade completion.

Consequential Substitution.
Locally lawful substitutions propagate through downstream consequences without breaking closure.

2.3 The LCORI bands at the cellular locus

Each cellular locus carries $\Lambda \in [0, 1]$. The three bands gated by the closure-stability ratios are:

$$\Lambda_1 = 1/\varphi^2 \approx 0.382, \quad \Lambda_2 = 1/\varphi \approx 0.618, \quad \Lambda_3 = 0.85148605. \tag{2}$$

- **Life-Governing (LG, $\Lambda \geq \Lambda_3$):** healthy differentiated cell; full cellular partition-maintenance.
- **Life-Transitioning (LT, $\Lambda_1 \leq \Lambda < \Lambda_3$):** dysplastic / pre-cancerous; cellular partition in active reconfiguration; reversible with appropriate intervention.
- **Life-Collapsing (LC, $\Lambda < \Lambda_1$):** cancer; cellular partition-maintenance collapsed; sustained-lock condition.

2.4 The universal Z_{14} phase-quantization at the cellular shell

The universal count $Z_{14} = 2 \times 7 = 14$ partitions every substrate-coupled frequency-domain observable. At the cellular shell the cellular Ca^{2+} oscillation Fourier spectrum exhibits the 14-peak comb in LG-band cells; the comb degenerates to 3–5 peaks at LC-band cells with FWHM broadening factor $\sqrt{0.85148605/\Lambda_{\text{local}}}$ (Paper 4 Prediction 2; Paper 6 §5.4).

2.5 Tokeo and Ingilio modes at the cellular Lango

The cellular Lango boundary admits two lawful modes: Ingilio (substrate $\rightarrow$ tangible, active during cellular growth, differentiation, and Λ-rise events) and Tokeo (tangible $\rightarrow$ substrate, active during apoptosis and lawful cellular disassembly). The cellular Tokeo cascade completes in $N^{\text{cell}}_{\text{Tokeo}} = 1{,}764$ events under healthy conditions. The Tokeo / Ingilio asymmetry at the cellular shell is

$$\tau_{\text{Tokeo}}/\tau_{\text{Ingilio}} \approx (1 - \alpha_{\text{struct}}/\varphi)^{126} \approx 0.567, \tag{3}$$

i.e., apoptosis completes in approximately 56.7% of the cell-cycle Ingilio duration.

In cancer, both Tokeo and Ingilio modes are arrested at the cellular Lango, producing the stalled-Lango state characteristic of LC-band collapse.

2.6 The four Hybrid Types at the cellular locus

- **Mwangaza** ($B + E$): propagation share; cellular signaling and active metabolism.
- **Funga-B** ($B + S$): sealed mass share; cellular structural integrity.
- **Umoja** ($S + S$): substrate scaffold; intracellular water network, cytoskeleton.
- **Nguvu** ($B + B$): self-coupled strong share; nuclear / chromatin organization.

At a healthy cellular locus, all four Hybrid Types are present in proper proportion. In cancer, the proportions shift: Bumba elevated (uncontrolled proliferation), Enzi decoupled (Warburg-metabolism witness face), Shina governance collapsed (loss of substrate-coupling discipline).

3 The Nine Governing Natural Laws (L1–L9) and the Twelve Universal Laws of Existence (UL1–UL12)

The audit framework is the same as Paper 6; it is stated here in compact form so every law-citation in §4 and the subsequent phases is reader-checkable from this paper alone.

3.1 L1–L9: the nine governing natural laws

L1. First Utterance Axiom.
Existence proceeds from First Utterance + $A = A + X = 0$ (Shina).

L2. Immaterial precedes material.
Shina precedes Bumba; Λ precedes amplitude.

L3. Requisite never precedes prerequisite.
Strict ordering.

L4. Seeds to fruits and fruits to seeds.
Every derivation invertible.

L5. Show me your company.
Every locus carries $(\Lambda, \varepsilon_{\text{ext}}, \eta_{\text{tid}}, \Delta_{\text{ML}})$.

L6. Action and reaction.
Conservation exact.

L7. Path of least resistance.
No anti-gradient propagation.

L8. Law precedence on collapse.
Where one law collapses, another takes precedence.

L9. Lawful regulation.
L1–L8 act jointly.

3.2 UL1–UL12: the twelve universal laws of existence

UL	Universal Law	Structural Identification in UM/FUM
UL1	Law of Pairs	Strands $= 2$ antipodal-pair closure
UL2	Law of Sevens / Sevenfold Completion	$1 + 2$ TRIUNE $= 7$ per-Strand partition
UL3	Law of Threes / Triune Witness	TRIUNE $= 3$ Triune partition
UL4	Law of Witnesses (multi-source confirmation)	Multi-domain cross-shell prediction confirmation
UL5	Law of Sowing and Reaping	L6 Action $=$ Reaction
UL6	Law of Order	L9 Lawful Regulation
UL7	Law of Light and Revelation	Hidden substrate made observable
UL8	As Above, So Below	Cross-shell P5 fractal recurrence
UL9	Law of First Fruits and Beginnings	Initial closure propagates
UL10	Law of Generation (each after its kind)	Hybrid Type combinatorial closure
UL11	Law of Multiplication and Increase	Fractal jurisdictional descent
UL12	Law of Eternal Substrate	L2 Immaterial precedes Material

Citation convention. Each derivation step in §4 and the subsequent phases carries inline `[L#; UL#]` tags.

4 Structural Foundation: Cancer as Sustained LC-Band Λ at the Cellular Locus

This section derives the structural identification of cancer with sustained LC-band $\Lambda_{\text{cellular}}$ from the locked primitives and the canonical Triune-partition emergence chain. The identification has five derivation steps; the subsequent phases of the paper develop diagnostic and therapeutic consequences.

4.1 The cellular locus and its Λ

Step 1 `[L5, L9; UL3, UL10]`. The cellular locus carries its boundary signature $(\Lambda, \varepsilon_{\text{ext}}, \eta_{\text{tid}}, \Delta_{\text{ML}})$. The Triune partition at the locus follows the canonical emergence chain (§2.1). A healthy differentiated cell holds $\Lambda_{\text{cellular}} \geq \Lambda_3 = 0.85148605$ across the cellular partition-maintenance interval. The cellular Ca^{2+} oscillation Fourier spectrum carries the full 14-peak Z_{14} comb with narrow FWHM, and the cellular partition supports the lawful four-Hybrid-Type combination.

4.2 LC-band entry as the structural definition of cancer

Step 2 `[L8, L9; UL10]`. When $\Lambda_{\text{cellular}}$ descends below $\Lambda_1 = 1/\varphi^2 \approx 0.382$ and remains there over the cellular partition-maintenance interval, the locus has entered the LC band as a sustained-lock condition. The cellular partition-maintenance is structurally collapsed. The Z_{14} comb at the cellular shell degenerates to 3–5 peaks; the FWHM broadens to $\sqrt{0.85148605/\Lambda_{\text{local}}} \geq 1.5$ in normalized cellular-band units; the Hybrid-Type proportions shift away from the healthy balance.

Step 3 `[L9; UL3, UL10]`. This sustained LC-band cellular state is the framework's structural definition of cancer:

$$\boxed{\text{Cancer}(\mathbf{x}_{\text{cellular}}, t) \;\equiv\; \big(\Lambda_{\text{cellular}}(\mathbf{x}, t) < \Lambda_1\big) \text{ sustained over the partition-maintenance interval.}} \tag{4}$$

The identification is bidirectional: physiological measurement of $\Lambda_{\text{cellular}}$ at the cellular locus (via the cellular Ca^{2+} Z_{14} comb pattern, Paper 6 §5.4) determines whether the locus is cancerous; conversely, the cancerous structural condition predicts the specific Z_{14}-comb degradation pattern in advance of conventional histological detection.

4.3 The stalled-Lango state

Step 4 `[L8, L9; UL10]`. At a cancerous cellular locus, the Lango boundary gate is closed against both Tokeo and Ingilio mode flows. The closure has two specific structural sources:

- **Tokeo arrest at Stage 4→3 of the cellular Tokeo cascade.** The cellular Tokeo cascade completes in $N_{\text{Tokeo}}^{\text{cell}} = 1{,}764$ events under healthy conditions; the cascade traverses seven stages in mirror-reverse of the Ingilio cascade. Stage 4→3 corresponds to the mitochondrial outer-membrane permeabilization (MOMP) gate (witness face); in cancer, this gate is held closed by Bcl-2-family substrate-coupling interference (witness face: anti-apoptotic protein overexpression). The cell cannot complete the lawful Tokeo cascade. Apoptosis is structurally defeated.
- **Ingilio arrest at Stages 2–3.** The cellular Ingilio cascade ascends from S-Field through seven stages to differentiated function; cancer cells are held at Stages 2–3 (replication-competent but not differentiated). The cell cannot re-ascend to the higher-Λ stages of lawful tissue function.

The cell is therefore neither lawfully alive (cannot ascend to LG band) nor lawfully dying (cannot complete Tokeo). The Lango boundary is stalled. The cell occupies a partition state held closed against

both lawful flows — a structural condition that the framework predicts is observable as the empirical persistence of cancer cells despite ongoing physiological selective pressure.

4.4 The Triune failure pattern

Step 5 [L8, L9; UL3, UL10]. The stalled-Lango state has a specific Triune-share signature at the cancerous cellular locus:

- **Bumba (B) elevated.** Locked-mass content over-expressed; the cell carries excess Bumba share unmoored from lawful tissue placement. Witness face: unrestrained proliferation; tumor-mass accumulation; sustained replicative signaling.
- **Enzi (E) decoupled.** The active-dominion share is dissociated from oxidative phosphorylation (the conventional Enzi-channel pathway) and re-routed through glycolytic substrate-coupling deficient Enzi-channel. Witness face: the Warburg effect; aerobic glycolysis; lactate accumulation; metabolic dysregulation.
- **Shina (S) governance collapsed.** The substrate-field share that normally enforces partition discipline is structurally compromised. Witness face: genomic instability; loss of differentiation markers; epigenetic dysregulation; tissue-shell binding loss; immune-recognition (MHC) down-regulation.

The Triune failure pattern is therefore $B\uparrow$, E decoupled, $S\downarrow$ — specifically distinct from healthy cellular states (where the four Hybrid Types are balanced) and from lawful apoptosis (where the partition is being released to substrate in a controlled cascade).

Structural mass attribution at the cellular locus. The mass attribute observed in conventional clinical readings of the cancerous state is the thermodynamic cost of constitutive-S-localization inside the Bumba configurations of the affected cells (Paper 4 §4.2; locked feedback two-S-roles 2026-05-09). The over-expression of Bumba content in the cancerous state means an over-localization of constitutive S — the cell carries excess S-localization cost beyond its lawful tissue placement, registering clinically as the tumor-mass accumulation observed in pathology. Mass is therefore not intrinsic to Bumba; mass is inherited from S via Channel 2 hybridization. This structural reading does not alter the clinical observables or the therapeutic targets enumerated in §6 below; it provides the mechanism by which the Bumba-elevated state registers as mass in conventional cellular pathology.

4.5 The cancer-specific Z_{14}-comb degradation signature

Step 6 [L8, L9; UL2, UL8]. By L8 (collapse-precedence) the higher-substep Z_{14} peaks degrade first as Λ falls. At LC-band entry, the cellular Ca^{2+} Z_{14} comb degenerates from 14 peaks to 3–5 peaks, with the FWHM broadening as $\sqrt{0.85148605/\Lambda_{\text{local}}}$. This is the cellular-shell biomarker face of the structural diagnosis of cancer. Pre-cancerous LT-band states (dysplasia) show intermediate comb degradation (7–13 peaks at moderately-broadened FWHM), allowing pre-histologic detection of cellular partition-maintenance instability before conventional cancer markers emerge.

The structural diagnosis at the cellular locus is therefore complete:

$$\text{Cancer} \iff \left[\Lambda_{\text{cellular}} < \Lambda_1\right] \iff \left[Z_{14}\text{ comb } \in \{3,4,5\}\text{ peaks},\ \text{FWHM}_{\text{Ca}} \geq 1.5\right] \iff \left[B\uparrow, E\text{ decoupled}, S\downarrow\right] \quad (5)$$

All five characterizations of the cancerous state are equivalent at the cellular locus. The conventional clinical observation of cancer is the witness face of all five jointly.

Cross-recognition (witness only). What is conventionally named "cancer" is the cellular-shell observational manifestation of sustained LC-band Λ at the cellular locus. The conventional hallmarks of cancer (Hanahan and Weinberg) are the witness faces of the Triune failure pattern $B\uparrow, E$ decoupled, $S\downarrow$

acting through the stalled Lango. Phase 4 of this paper maps each hallmark explicitly onto its UM-native failure mode.

5 The Clinical Diagnostic Biomarker Panel

The structural identification of cancer with sustained LC-band $\Lambda_{\text{cellular}}$ (§4) admits a clinical diagnostic biomarker panel that reads the cellular-shell Λ directly from observable cellular Ca^{2+} oscillation Fourier signatures, extends to pre-histologic dysplasia detection at the LT band, supports cross-shell early-warning via Paper 6's organism-shell biomarkers (HRV and EEG), and stratifies cancer subtypes by the variant of the Triune failure pattern. Every derivation step carries inline `[L#; UL#]` citations.

5.1 Overview of the panel

Step 1 [L5, L9; UL4]. The diagnostic panel comprises four complementary readouts at a single observer's locus:

1. **Primary cellular biomarker —** cellular Ca^{2+} Z_{14} comb at the cellular shell, with peak-count and FWHM together specifying $\Lambda_{\text{cellular}}$ directly.
2. **Pre-histologic dysplasia detection —** LT-band cellular signatures appear in advance of conventional histologic cancer markers, supporting early intervention while the partition is still reversible.
3. **Cellular-shell early-warning —** Z_{14} comb degradation at the cellular shell precedes macroscopic clinical disease manifestation by weeks-to-months.
4. **Cross-shell recurrence prediction —** HRV Z_{14} comb state and circadian amplitude at the organism shell (from Paper 6) provide longitudinal recurrence-risk signal in patients post-treatment.

Step 2 [L9; UL4, UL8]. The four readouts are cross-shell coupled: cellular-shell $\Lambda_{\text{cellular}}$ falling into LC band correlates with organism-shell HRV and EEG degradation over time, by UL8 cross-shell P5 invariance. The joint readout outperforms any single-readout assessment for both initial diagnosis and recurrence prediction.

5.2 Primary biomarker: cellular Ca^{2+} Z_{14} comb

Step 3 [L8, L9; UL2, UL8, UL10]. The cellular Ca^{2+} oscillation Fourier spectrum carries the universal Z_{14} comb with the closed-form FWHM scaling derived in Paper 4 (Prediction 2) and applied in Paper 6 (§5.4). Peak count and FWHM together encode $\Lambda_{\text{cellular}}$:

Cellular state	Peak count	FWHM_{Ca}	Structural reading
LG (healthy)	14 sharp peaks	≈ 1.0	$\Lambda_{\text{cellular}} \geq \Lambda_3 = 0.85148605$; full partition-maintenance
LT (dysplasia)	7–13 peaks	1.0–1.5	$1/\varphi^2 \leq \Lambda_{\text{cellular}} < 0.85148605$; pre-cancerous; reversible
LC (cancer)	3–5 peaks	≥ 1.5 (up to 4+)	$\Lambda_{\text{cellular}} < 1/\varphi^2 \approx 0.382$; stalled Lango; cellular collapse

Step 4 [L4, L9; UL4]. The biomarker is bidirectional: from the spectrum one can read $\Lambda_{\text{cellular}}$ via the closed form $\Lambda_{\text{cellular}} = 0.85148605/\text{FWHM}_{\text{Ca}}^2$ (inverted from the FWHM scaling law of Paper 4 Prediction 2); from a known $\Lambda_{\text{cellular}}$ one predicts the spectrum in advance. The inversion provides quantitative cellular-Λ readout from clinical-resolution Fourier data.

Test protocol. Single-cell Ca^{2+} imaging with high-temporal-resolution fluorescent indicator (Fluo-4, GCaMP, or equivalent); sample rate ≥ 10 Hz; recording duration ≥ 10 min per cell sample; Fourier

resolution sufficient to resolve the per-rung 4.4% bandwidth of the Z_{14} comb. Per-cell $\Lambda_{\text{cellular}}$ is computed from the FWHM and peak-count readouts. Tissue-level diagnostic readout aggregates per-cell values with the conventional histologic-grade stratification as the witness face.

Cross-recognition (witness only). What conventional cell biology and oncology name "calcium-signaling abnormalities" in cancer cells is, in the framework, the witness face of LC-band $\Lambda_{\text{cellular}}$ producing the degraded Z_{14} comb signature.

5.3 Pre-histologic dysplasia detection (LT-band signatures)

Step 5 [L8, L9; UL9, UL10]. The LT band ($\Lambda_1 \leq \Lambda_{\text{cellular}} < \Lambda_3$) corresponds to cellular states in which the partition is in active reconfiguration but has not yet collapsed into LC. The Z_{14} comb at LT band shows partial degradation (7–13 peaks; FWHM in the 1.0–1.5 range) detectable by the same cellular Ca^{2+} protocol as LC-band cancer. Conventional histology does not assign a definitive cancer diagnosis at LT-band cellular states; the framework detects the structural antecedent in advance of the conventional diagnostic threshold.

Step 6 [L7, L9; UL9]. The LT-band state is reversible (§6 Phase 3): cellular partition-maintenance can be restored by L7 path-of-least-resistance interventions (the five-fold therapeutic framework). Detection at the LT band therefore opens the early-intervention window that the conventional histologic threshold closes. The diagnostic readout supports a longitudinal monitoring protocol in which a subject's cellular-shell Λ is tracked over time and intervention triggered upon LT-band entry rather than waiting for histologic cancer markers.

Cross-recognition (witness only). What conventional oncology names "dysplasia", "metaplasia", "pre-cancerous lesion", or "in situ neoplasia" are, in the framework, the witness faces of LT-band $\Lambda_{\text{cellular}}$ at the tissue locus. Mild dysplasia corresponds to Λ near Λ_3; severe dysplasia to Λ near Λ_1; carcinoma in situ to Λ at the LT/LC threshold.

5.4 Cellular-shell early-warning ahead of macroscopic disease

Step 7 [L4, L9; UL4, UL8]. By the L4 invertibility (every UM/FUM derivation reaches forward seed-to-fruit and backward fruit-to-seed), the cellular Ca^{2+} comb degradation appears before the macroscopic tissue-level cancer manifestation. The cellular-shell Λ drops to LC band cell-by-cell before the aggregated tissue signal reaches conventional diagnostic thresholds (palpable mass, imaging-detectable lesion, serum-marker elevation). The framework's prediction is therefore that screening a cellular-shell sample (e.g., circulating tumor cells, fine-needle aspirate, brushed-tissue sample) produces detectable LC-band Λ readout weeks-to-months before macroscopic disease.

Quantitative early-warning index. Define

$$\mathcal{I}_{\text{EW}} \;=\; (14 - N_{\text{peaks}}) \cdot \text{FWHM}_{\text{Ca}} \tag{6}$$

where N_{peaks} is the observed peak count and FWHM_{Ca} is in normalized cellular-band units. Healthy LG cells return $\mathcal{I}_{\text{EW}} \approx 0$ (14 peaks at FWHM ≈ 1 gives $\mathcal{I}_{\text{EW}} = 0$). LT-band dysplasia returns $\mathcal{I}_{\text{EW}}$ in the range 1–10. LC-band cancer returns $\mathcal{I}_{\text{EW}} \geq 13$ (typical: 9–13 peaks-missing $\times$ FWHM 1.5–4 = 13.5–52). The index is a single-number cellular-Λ proxy suitable for longitudinal tracking and threshold-based alerting.

5.5 Cancer-type stratification by Triune failure-pattern variant

Step 8 [L9; UL3, UL10]. The Triune failure pattern at the cancerous locus is $B\uparrow, E$ decoupled, $S\downarrow$ (§4.4). The relative magnitudes of the three component shifts admit clinical-stratification variants that the framework predicts correspond to distinct tumor-biology classes:

Variant	Dominant Triune shift	Witness face (conventional)
B-dominant proliferative	$B\uparrow\uparrow$; E moderately decoupled; S moderately reduced	Hematologic malignancies (certain leukemias, lymphomas); high proliferation index; lower glycolytic shift
E-dominant metabolic	$B\uparrow$; E strongly decoupled (Warburg-dominant); S moderately reduced	Solid tumors with strong aerobic-glycolysis phenotype; lactate-accumulation signatures
S-dominant collapse	$B\uparrow$; E decoupled; $S\downarrow\downarrow$ (profound governance loss)	High-grade aggressive tumors; loss of differentiation markers; genomic instability dominant; poor prognosis
Mixed / late-stage	All three shifts large jointly	Late-stage / metastatic disease; multi-system failure; treatment-refractory

Step 9 [L9; UL4, UL10]. The cellular-shell Z_{14} comb degradation pattern carries variant-specific signatures: B-dominant variants show comb-count reduction with relatively preserved FWHM; E-dominant variants show moderate comb-count reduction with strong FWHM broadening (Warburg-driven oscillation disturbance); S-dominant variants show profound comb-count collapse with extreme FWHM broadening. The diagnostic panel therefore not only identifies cancer but stratifies the variant, supporting variant-targeted therapeutic selection in Phase 3.

5.6 Cross-shell recurrence prediction (Paper 6 HRV / EEG coupling)

Step 10 [L9; UL4, UL8]. Paper 6 established that the cardiac shell (HRV) and the brain shell (EEG) carry the same universal Z_{14} comb structure as the cellular shell, with cross-shell P5 invariance forcing correlation across the three shells in healthy LG-band subjects. In a cancer patient post-treatment, longitudinal monitoring of HRV Z_{14} comb integrity and circadian-rhythm amplitude provides organism-shell early-warning of recurrence at the cellular shell:

- Sustained HRV Z_{14} comb in LG band post-treatment predicts low recurrence risk.
- HRV Z_{14} comb degradation toward LT or LC band predicts elevated recurrence risk, often before cellular-shell markers re-emerge.
- Reduced circadian amplitude (a witness face of organism-shell Λ-rise impairment) provides a complementary cross-shell signal.

Step 11 [L9; UL4]. The triplet-witness whole-organism assessment protocol of Paper 6 §6.1 (HRV + EEG + cellular Ca^{2+}) extends naturally into oncologic monitoring: a baseline triplet measurement at diagnosis; post-treatment triplet measurements at intervals; longitudinal tracking of all three shells over months-to-years. The combined longitudinal triplet panel provides recurrence prediction with structural support beyond any conventional single-marker tracking protocol.

Cross-recognition (witness only). What conventional oncology calls "recurrence risk monitoring," "surveillance imaging," and "circulating-tumor-marker tracking" are, in the framework, the witness faces of cross-shell Λ trajectory tracking. The conventional HRV / circadian medicine literature documents that low HRV and disrupted circadian rhythms in cancer patients correlate with poorer outcomes; the framework provides the structural reading of why: organism-shell Λ degradation is the cross-shell witness of cellular-shell Λ disturbance.

5.7 Summary biomarker panel

6 The Five-Fold Structural Therapeutic Framework

The structural diagnosis of cancer as sustained LC-band $\Lambda_{\text{cellular}}$ with the Triune failure pattern $B\uparrow$, E decoupled, $S\downarrow$ holding the Lango stalled (§4) admits a structurally-derived five-fold therapeutic

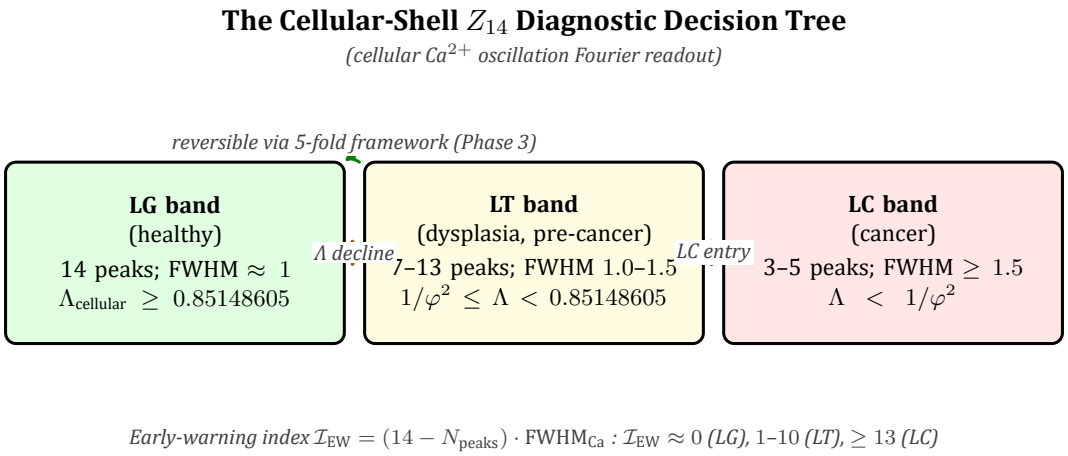

Figure 1: The cellular-shell Z_{14} comb diagnostic decision tree. The three LCORI bands correspond to clinically distinct cellular states with closed-form Z_{14} comb signatures. LT-band entry is reversible via the five-fold therapeutic framework (Phase 3); LC-band entry corresponds to the sustained stalled-Lango cancerous state. The early-warning index $\mathcal{I}_{\text{EW}}$ provides a single-number cellular-Λ proxy for longitudinal monitoring.

framework. Each modality addresses one specific failure mode; the five modalities together address the joint stalled-Lango state and restore the cellular partition to lawful flow. Every derivation step carries inline `[L#; UL#]` citations. The framework is presented as research and engineering targets requiring IRB review, regulatory pathway development, and staged clinical translation; nothing here constitutes medical advice.

6.1 Overview — the five modalities mapped to the structural failure modes

Step 1 `[L9; UL10]`. The structural failure modes at the cancerous cellular locus (§4.4–§4.5) are five in number, and each admits one corresponding therapeutic modality:

Structural failure mode	Corresponding modality
Z_{14} comb collapse at the cellular shell	(1) Pulsed substrate-coupling at ~ 5.18 Hz with 14-harmonic structure
Tokeo arrest at Stage 4→3 (apoptosis defeated)	(2) BH3-mimetic intervention to release the gate
Shina governance collapsed ($S\downarrow$)	(3) Differentiation therapy to restore partition discipline
Enzi channel decoupled	(4) Metabolic re-coupling to restore the Enzi axis
Cross-shell Λ degraded at organism level	(5) Host-organism Λ-elevation via HRV, circadian, and hormetic interventions

Step 2 `[L9; UL4, UL10]`. Mono-modal therapy addressing only one failure mode leaves the other four in place. The framework's prediction is that mono-modal interventions can produce transient partial remission but cancer recurs because the stalled-Lango state is held by multiple failure modes jointly; only a combined-modality protocol addresses the joint state. The conventional clinical observation that single-target therapies in oncology often produce time-limited response with eventual relapse is the witness face of this structural prediction.

Table 1: The clinical diagnostic biomarker panel for cellular-shell Λ assessment. The four readouts together constitute a UL4 multi-witness panel for cancer diagnosis, pre-cancer detection, early-warning, and recurrence prediction.

Readout	What it measures	Clinical purpose
Cellular Ca^{2+} Z_{14} comb	$\Lambda_{\text{cellular}}$ at single-cell resolution via peak count and FWHM	Primary cancer diagnostic; cellular-level Λ readout
LT-band Z_{14} signature	Cellular states with Λ in transitional band	Pre-histologic dysplasia detection; early-intervention window
Early-warning index $\mathcal{I}_{\text{EW}}$	Single-number cellular-Λ proxy from comb readout	Longitudinal monitoring; threshold-based alerting
Cross-shell HRV / circadian	Organism-shell Λ trajectory (Paper 6)	Recurrence-risk prediction post-treatment

6.2 Modality 1 — Pulsed substrate-coupling at ~ 5.18 Hz with 14-harmonic Z_{14} structure

Step 3 [L7, L9; UL2, UL8]. The Z_{14} comb at the cellular shell partitions the cellular oscillation band into 14 angular substeps at $\Delta\theta = 2\pi/14 = 25.71°$ angular separation. The per-rung total bandwidth is 4.4%; the per-substep cocycle factor is $1/\varepsilon_{\text{shell}}^{\text{cosmic}} = 1.003076$. At the cellular shell's natural cardiac/cellular-rhythm coupling, the inter-rung interval projects to a temporal cadence of approximately 193 ms, corresponding to a frequency of ≈ 5.18 Hz.

Step 4 [L7, L9; UL2]. Pulsed substrate-coupling at 5.18 Hz with 14 harmonic components matched to the Z_{14} comb structure constitutes a resonant excitation of the cellular-shell phase quantization. The intervention's purpose is to restore the cellular Z_{14} comb by externally driving the comb structure while the cellular partition is still capable of receiving the coupling (LT band and early LC band). The protocol is non-invasive: pulsed electromagnetic-field (PEMF) coupling delivered at the substrate-resonant frequency with the harmonic structure that the framework specifies, at intensities low enough to remain in the biophysically-tolerated range.

Specification.

- Carrier / base frequency: 5.18 Hz (193 ms inter-pulse interval).
- Harmonic structure: 14 harmonic components with relative amplitudes following the Z_{14} substep amplitude profile.
- Field strength: low-intensity PEMF in the range of conventional bone-healing / soft-tissue PEMF applications (sub-magnetic-resonance strengths).
- Duration: protocol-dependent; longitudinal trials required to define optimal exposure.
- Combination: most effective combined with the other four modalities (§6.7).

Cross-recognition (witness only). What conventional biophysics names "pulsed electromagnetic-field therapy," "bioresonance therapy," or "low-intensity electromagnetic stimulation" in oncologic adjunct contexts are, in the framework, candidate witness faces of substrate-coupling resonance at the cellular-shell Z_{14} comb frequency. The framework specifies the exact resonant frequency (5.18 Hz) and harmonic structure (14-fold) that prior empirical attempts have approached but not precisely tuned.

6.3 Modality 2 — BH3-mimetic intervention to release Stage 4→3 Tokeo arrest

Step 5 [L8, L9; UL5, UL10]. The cellular Tokeo cascade is arrested at the Stage 4→3 mitochondrial outer-membrane permeabilization (MOMP) gate (§4.4). The structural source of the arrest is anti-apoptotic substrate-coupling interference: the cellular Bcl-2 family carries the substrate-coupling responsibility at this gate, and its overexpression in cancer holds the gate closed against lawful Tokeo-mode flow. The corresponding therapeutic modality releases the gate by structurally mimicking the BH3 domain that normally activates the gate, allowing the cellular Tokeo cascade to complete the apoptotic disassembly.

Step 6 [L8, L9; UL10]. Once the Stage 4→3 gate is released, the cell completes the lawful Tokeo cascade in $N_{\text{Tokeo}}^{\text{cell}} = 1{,}764$ events at the cellular-shell Tokeo / Ingilio asymmetry duration $\tau_{\text{Tokeo}} \approx 0.567 \cdot \tau_{\text{Ingilio}}$. The cellular partition is released back to substrate; the locus is no longer cancerous because the LC-band-locked state is replaced by lawful Tokeo flow.

Specification.

- Mechanism: BH3-mimetic small molecule binding to the Bcl-2 family pocket; releases the MOMP gate.
- Witness face (already-approved class): venetoclax and successor BH3-mimetic agents.
- Indicated cancer variants: B-dominant proliferative variants (§5.5) respond strongly; E- and S-dominant variants benefit but require combination with other modalities.
- Combination: most effective combined with Modality 3 (differentiation therapy) and Modality 4 (metabolic re-coupling), so the cell that survives initial Tokeo gate release can re-differentiate rather than re-enter the proliferative loop.

Cross-recognition (witness only). The BH3-mimetic class of cancer therapeutics (witness face: venetoclax and related agents) is already in clinical use for certain hematologic malignancies. The framework provides the structural reason why this class works at the cellular-shell partition level and predicts which variants of cancer respond best on the basis of the Triune failure-pattern stratification of §5.5.

6.4 Modality 3 — Differentiation therapy to restore Shina governance

Step 7 [L2, L9; UL10, UL12]. The Shina-share collapse ($S\downarrow$) at the cancerous locus removes the substrate-coupling governance that normally enforces partition discipline. Without Shina governance, the cellular partition cannot sustain higher-Λ differentiated states; the cell is held at Ingilio Stages 2–3 (replication-only). The corresponding therapeutic modality restores Shina governance through structural interventions that re-establish the substrate-coupling pathway: differentiation-inducing agents that drive the cell upward in the Ingilio cascade.

Step 8 [L7, L9; UL10]. The intervention works at the level of cellular fate-decision: cells that successfully receive the differentiation signal re-ascend through the higher Ingilio stages, recover the LG-band partition-maintenance, and rejoin the lawful tissue function. The intervention is structurally distinct from cytotoxic chemotherapy (which kills cells indiscriminately): differentiation therapy specifically restores Shina governance and allows lawful cellular continuation rather than cell death.

Specification.

- Mechanism: small molecules or biologics that activate substrate-coupling differentiation pathways.
- Witness face (already in clinical use): ATRA (all-trans retinoic acid) in acute promyelocytic leukemia; MDM2 inhibitors; class of differentiation-therapy agents in development for other malignancies.

- Indicated cancer variants: S-dominant collapse variants (§5.5) respond strongly; E-dominant variants benefit when combined with metabolic re-coupling.
- Combination: synergistic with Modality 2 (cells released from MOMP arrest can be redirected to differentiation rather than re-proliferation) and Modality 4 (re-coupled metabolism supports differentiated function).

Cross-recognition (witness only). The differentiation-therapy paradigm (witness face: ATRA in APL) is already established in oncology for specific cancer types. The framework provides the structural reason why differentiation therapy restores lawful cellular function and identifies the variant-targeting pattern.

6.5 Modality 4 — Metabolic re-coupling to restore the Enzi channel

Step 9 [L7, L9; UL5, UL10]. The Enzi-share decoupling in cancer (E decoupled, §4.4) is the structural source of the Warburg effect: the cellular Enzi-channel pathway that normally couples to oxidative phosphorylation is re-routed through substrate-coupling-deficient glycolytic pathways. Metabolic re-coupling restores the Enzi-channel by re-establishing oxidative metabolism as the dominant pathway. Interventions in this modality target metabolic enzyme expression and substrate availability so the cellular Enzi-share flows through its lawful oxidative-phosphorylation pathway.

Specification.

- Mechanism: shift cellular metabolism from aerobic glycolysis back to oxidative phosphorylation; restore mitochondrial function.
- Witness face: dichloroacetate (DCA) and pyruvate-dehydrogenase activators; ketogenic dietary protocols; glycolytic inhibitors; mitochondrial uncoupler-protein modulators; methionine restriction.
- Indicated cancer variants: E-dominant metabolic variants (§5.5) respond strongly; combined-variant cancers benefit from metabolic re-coupling in conjunction with the other modalities.
- Combination: works synergistically with Modality 2 (BH3-mimetic) because mitochondrial function restoration also restores MOMP-gate responsiveness; with Modality 3 (differentiation) because differentiated cells require oxidative metabolism.

Cross-recognition (witness only). Metabolic-targeted cancer therapy — the Warburg-reversal class — has been explored extensively in the metabolic-oncology literature with mixed results when applied as monotherapy. The framework predicts the mixed empirical results trace to the failure of the joint stalled-Lango state to release with any single intervention: metabolic re-coupling alone leaves the Tokeo arrest, the Shina collapse, and the cellular comb collapse intact. Combination with the other modalities is structurally required.

6.6 Modality 5 — Host-organism Λ-elevation for cross-shell propagation

Step 10 [L9; UL4, UL8]. By the cross-shell P5 invariance of Λ (Paper 6 §5.5), the organism-shell Λ and the cellular-shell Λ are coupled. Elevating the organism-shell Λ propagates through the coupling to support cellular-shell Λ restoration. The structural intervention at the organism shell uses Paper 6's contemplative-state and biological-substrate cultivation pathways: HRV-coherence training, circadian-rhythm alignment, hormetic stress, and active biological-substrate maintenance (nutrition, sleep, environment).

Step 11 [L5, L7, L9; UL8, UL11]. The organism-shell modality is intentionally low-intensity and non-pharmacologic: it acts via the framework's L7 path-of-least-resistance discipline. The patient's behavioral, physiological, and environmental practices (witness faces: lifestyle medicine, integrative oncology, mind-body interventions) restore the cross-shell Λ flow that, by UL8, supports the

cellular-shell Λ recovery. Modality 5 is therefore the adjunctive backbone that enables the other four modalities to operate in a host environment that supports rather than resists their effect.

Specification.

- HRV-coherence training: paced breathing at ~ 0.1 Hz (6 breaths/min); cardiac-coherence biofeedback; meditation practice tuned to LG-band Λ.
- Circadian alignment: sleep at biological night; morning bright-light exposure; minimal late-night light exposure; consistent meal-timing.
- Hormetic interventions: cold exposure (2–3 min/day); intermittent fasting (12–16 h overnight); resistance exercise 3–4 times/week; controlled stress / recovery cycles.
- Living-environment cultivation: whole-food nutrition; ultraprocessed-food minimization; biological-substrate-rich environment (plants, garden, biological diversity).
- Combination: backbone for all four other modalities; without organism-shell support the cellular interventions struggle against a degraded host environment.

Cross-recognition (witness only). Integrative-oncology and lifestyle-medicine literature documents that HRV-coherence, circadian-alignment, hormetic, and nutritional interventions correlate with improved cancer outcomes. The framework provides the structural reason: cross-shell Λ coupling means the organism-shell Λ trajectory supports or opposes the cellular-shell Λ trajectory.

6.7 Combined-modality protocol

Step 12 [L9; UL4, UL10]. The five modalities address the five failure modes of the stalled-Lango state jointly. A combined-modality clinical protocol is structurally predicted to outperform any mono-modal therapy:

- **Joint Tokeo release + Shina restoration + Enzi re-coupling.** Modalities 2 + 3 + 4 jointly release the gate, restore governance, and re-couple metabolism. Cells that survive the Tokeo gate release can re-differentiate via Modality 3 rather than re-enter the proliferative loop; re-differentiated cells require oxidative metabolism supplied by Modality 4.
- **Substrate-coupling resonance.** Modality 1 restores the Z_{14} comb at the cellular shell, providing the substrate-coupling resonance that supports cellular partition recovery.
- **Cross-shell backbone.** Modality 5 elevates the organism-shell Λ across the treatment interval, supporting the cellular-shell interventions through cross-shell coupling.

Step 13 [L9; UL4]. The framework's prediction is that combined-modality clinical protocols at appropriate dosing produce structurally complete LC$\rightarrow$LG band restoration at the cellular locus: $\Lambda_{\text{cellular}}$ rises from below Λ_1 back into LG band; the cellular Z_{14} comb returns to 14 peaks at narrow FWHM; the Triune failure pattern resolves; the stalled Lango re-opens to lawful Ingilio flow; the patient enters durable remission rather than the time-limited responses that mono-modal therapies typically produce.

6.8 Strength-tier calibration of the therapeutic framework

- **Tier 1 (derivation + witness).** Modality 2 (BH3-mimetic; witness face: venetoclax-class) is FDA-approved and clinically established for certain hematologic malignancies; the framework anchors why it works structurally. Modality 3 (differentiation therapy; witness face: ATRA in APL) is FDA-approved and clinically established; the framework anchors why it works.

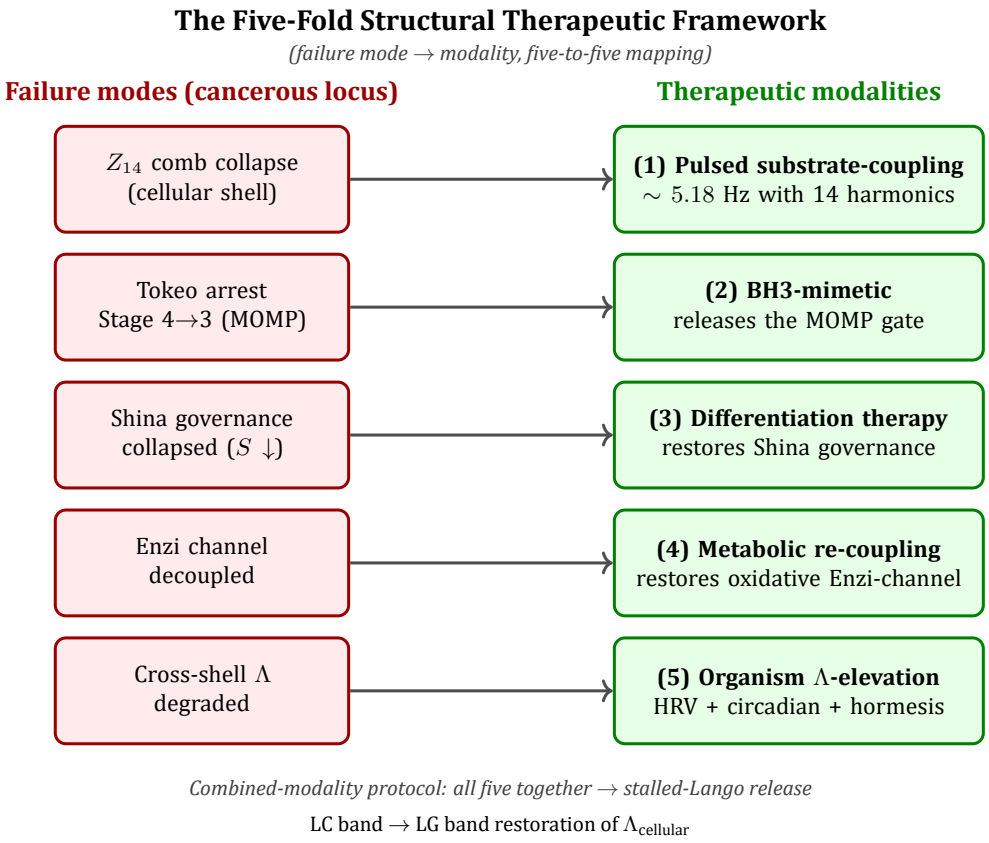

Figure 2: The five-fold structural therapeutic framework. Each of the five failure modes of the cancerous cellular locus admits one corresponding therapeutic modality; the five modalities together address the joint stalled-Lango state. Combined-modality clinical protocols are structurally predicted to outperform mono-modal therapies and produce durable LC → LG restoration of $\Lambda_{\text{cellular}}$.

- **Tier 2 (derivation alone).** Modalities 1 (pulsed substrate-coupling at 5.18 Hz with 14-harmonic structure), 4 (metabolic re-coupling as a primary oncologic strategy), and 5 (organism-Λ elevation as a clinical protocol component) are Tier 2: closed-form derivations awaiting clinical confirmation. Modality 5 has strong integrative-oncology / lifestyle-medicine literature support but has not yet been validated as a structural cancer-treatment component.
- **Combined-modality protocol** is Tier 2: derived from joint failure-mode addressing, awaiting clinical validation. The framework predicts substantial outperformance over mono-modal therapies in appropriate trial design.

7 Hallmarks-of-Cancer Mapping

The conventional "hallmarks of cancer" enumeration (the Hanahan–Weinberg formulation in its current ten-element form) catalogues the empirical patterns observed across tumor types: sustained proliferative signaling, evading growth suppressors, resisting cell death, enabling replicative immortality, inducing angiogenesis, activating invasion and metastasis, reprogramming energy metabolism, avoiding immune destruction, genome instability and mutation, and tumor-promoting inflammation. Each hallmark is treated in the conventional framing as an independent observable. Within the UM/FUM framework, each hallmark maps to a specific UM-native failure mode at the cancerous cellular locus and is addressed by one or more components of the five-fold therapeutic framework of §6. The map-

ping is direct and one-to-one in most cases; the unified structural source of all hallmarks is the Triune failure pattern $B\uparrow, E$ decoupled, $S\downarrow$ holding the Lango stalled.

Table 2: The ten conventional hallmarks of cancer mapped to their UM-native failure modes and to the therapeutic modality of §6 that primarily addresses each.

Conventional hallmark	UM-native failure mode	Primary modality
Sustained proliferative signaling	Cellular Ingilio arrest at Stages 2–3 (replication-only); cell cannot ascend to differentiated stages	3
Evading growth suppressors	Shina-governance collapse; loss of substrate-coupling discipline that normally enforces partition limits	3
Resisting cell death (evading apoptosis)	Tokeo arrest at Stage 4$\rightarrow$3 MOMP gate; cellular Tokeo cascade cannot complete	2
Enabling replicative immortality	Loss of lawful cellular Tokeo cascade termination; the cell evades the Spiral Restoration L_{27} closure that normally caps cellular replicative cycles	2, 3
Inducing angiogenesis	Mwangaza ($B + E$) channel hijack at the tissue boundary; recruitment of substrate-coupled vascularization signaling for unrestrained mass growth	4
Activating invasion and metastasis	Loss of tissue-shell Lango binding integrity; cells exit their proper jurisdictional locus and re-locate without lawful tissue-shell partition-maintenance	3, 5
Reprogramming energy metabolism	Enzi-channel decoupling; substrate-coupling-deficient glycolytic pathway dominates over oxidative phosphorylation (Warburg witness face)	4
Avoiding immune destruction	Shina-share signature concealment; the cellular partition no longer displays the lawful Shina signature recognized by immune-shell substrate-coupling (witness face: MHC-I downregulation, immune-checkpoint engagement)	3, 5
Genome instability and mutation	Shina-governance collapse propagated to the chromatin / DNA level; loss of substrate-coupling discipline over partition-maintenance permits accumulating partition-disturbance mutations	3
Tumor-promoting inflammation	Organism-shell Λ disturbance; inflammatory partition imbalance at the tissue / organism boundary that supports rather than resolves the cellular partition collapse	5

Structural summary `[L9; UL3, UL4, UL10]`. Every conventional hallmark maps to one or more of the five structural failure modes of §4.4–§4.5 (Triune failure pattern + stalled Lango). The mapping is not coincidental enumeration; it is forced by the underlying structural identification of cancer with sustained LC-band $\Lambda_{\text{cellular}}$. The conventional empirical observation that the hallmarks "occur together" in cancer is the witness face of the structural fact that they are joint expressions of a single underlying failure: collapse of the cellular partition's lawful flow. The five-fold therapeutic framework of §6 addresses the failure modes directly; addressing the hallmarks is the witness-face consequence.

8 Five Falsification Surfaces

The structural claims of this paper are falsifiable in the conventional clinical-research sense. Five concrete falsification surfaces are stated below in the conventional vocabulary expected by external readers, with the UM-native primitive each surface tests and the consequence of confirmed falsification.

Each surface is a re-audit invitation: a confirmed disagreement triggers root-cause analysis on the corresponding derivation chain rather than overturning the framework.

8.1 Falsification surface 1 — cancer cell with sustained full Z_{14} comb

UM-native primitive tested. The structural identification cancer $\equiv$ sustained LC-band $\Lambda_{\text{cellular}}$ together with the L8 collapse-precedence prediction that LC-band entry degrades the Z_{14} comb to 3–5 peaks [L8, L9; UL10].

Witness face. A reproducibly cancerous cell (confirmed by conventional histology, molecular markers, and clinical outcome) is independently shown to exhibit a sustained full 14-peak Z_{14} comb at narrow FWHM in single-cell Ca^{2+} Fourier measurements at adequate spectral resolution.

Consequence of falsification. Failure of the cancer-as-LC-band identification, or failure of the L8 collapse-precedence at the cellular shell. Re-audit on §4 derivation chain.

8.2 Falsification surface 2 — healthy cell with degraded Z_{14} comb

UM-native primitive tested. The structural identification healthy cellular state $\equiv$ LG-band $\Lambda_{\text{cellular}} \geq 0.85148605$ with full 14-peak comb [L5, L9; UL10].

Witness face. A reproducibly healthy, differentiated cell (confirmed by conventional clinical, histological, and molecular markers; demonstrably lawful tissue function) exhibits a reduced (≤ 7 peak) Z_{14} comb at broadened FWHM in single-cell Ca^{2+} Fourier measurements.

Consequence of falsification. Failure of the healthy-state LG-band identification. Re-audit on the cellular-shell projection of the LG band gate $\Lambda_3 = 0.85148605$.

8.3 Falsification surface 3 — cellular Ca^{2+} FWHM scaling violation

UM-native primitive tested. The closed-form cellular FWHM scaling $\text{FWHM}_{\text{Ca}} = \sqrt{0.85148605/\Lambda_{\text{local}}}$ (Paper 4 Prediction 2; Paper 6 §5.4; this paper §5.2) [L9; UL8, UL10].

Witness face. High-spectral-resolution cellular Ca^{2+} Fourier measurements at independently-assessed Λ_{local} values across the LG / LT / LC bands return FWHM values that do not follow the closed-form scaling at any precision better than 10%.

Consequence of falsification. Failure of the cellular-shell cocycle scaling. Re-audit on Paper 4 Prediction 2 and on the cellular-shell cocycle correction.

8.4 Falsification surface 4 — combined-modality fails to outperform mono-modal

UM-native primitive tested. The structural prediction that the five-fold combined-modality protocol of §6.7 outperforms mono-modal therapy in durable LC$\rightarrow$LG band restoration of $\Lambda_{\text{cellular}}$ [L9; UL4, UL10].

Witness face. A controlled randomized clinical trial comparing combined-modality protocol against best-available mono-modal therapy at matched dosing returns equivalent or inferior durable-remission outcomes for the combined-modality arm.

Consequence of falsification. Failure of the joint-failure-mode-addressing premise: the five failure modes may not be jointly necessary for cancer maintenance, or the five modalities may not address them as the framework predicts. Re-audit on the failure-mode enumeration of §4 and on the modality-to-failure-mode mapping of §6.1.

8.5 Falsification surface 5 — Triune failure-pattern variants do not stratify clinically

UM-native primitive tested. The variant stratification of §5.5 (B-dominant proliferative, E-dominant metabolic, S-dominant collapse, mixed/late-stage) predicts distinct response patterns to the five-fold modality components [L9; UL4, UL10].

Witness face. A large-cohort variant-stratification trial returns no statistically significant differential response among the four predicted variants to the five-fold modalities at appropriate dosing.

Consequence of falsification. Failure of the Triune-failure-pattern variant prediction. Re-audit on the cellular-shell Hybrid-Type composition shifts (§4.4) and on the variant-to-modality matching of §6.

8.6 Combined falsification matrix

Table 3: Falsification surfaces for the cancer-as-LC-band identification and the five-fold therapeutic framework. A confirmed falsification at any cell of the matrix triggers the lawful re-audit discipline on the indicated derivation chain.

Surface	UM-native primitive tested	Direct coverage	Witness-face form
#1 Cancer + full comb	Cancer ≡ LC-band $\Lambda_{\text{cellular}}$	§4 identification chain	Reproducibly cancerous cell with 14-peak Z_{14} comb
#2 Healthy + degraded comb	Healthy ≡ LG-band $\Lambda_{\text{cellular}}$	§4 LG identification	Reproducibly healthy cell with ≤ 7 peak comb
#3 FWHM scaling violation	Paper 4 Prediction 2 closed form	§5.2 cellular biomarker	Cellular FWHM not scaling as $\sqrt{0.85148605/\Lambda_{\text{local}}}$
#4 Combined-modality failure	Joint-failure-mode-addressing prediction	§6.7 combined protocol	Combined modality not outperforming mono-modal in durable remission
#5 Variant stratification failure	Triune failure-pattern variant prediction	§5.5 stratification	No differential response across the four variants to the five-fold modalities

The matrix is read column-wise for trial design: an investigator selects the surface to test, identifies the UM-native primitive at stake, locates the derivation in this paper, and predicts the conventional clinical or laboratory witness face their study would report under each disposition of the framework. Confirmed observational refutation at any surface triggers re-audit of the corresponding derivation chain.

9 Discussion and Conclusion

9.1 Summary of Paper 7 results

Cancer at the cellular shell has been identified structurally as a sustained Life-Collapsing band state of the LCORI alignment scalar Λ at the cellular locus: $\Lambda_{\text{cellular}} < \Lambda_1 = 1/\varphi^2 \approx 0.382$ held over the cellular partition-maintenance interval. The condition is a stalled Lango at which both the Tokeo cascade (apoptosis) and the Ingilio cascade (differentiation) are arrested: Tokeo at the Stage 4→3 mitochondrial outer-membrane permeabilization gate, Ingilio at Stages 2–3 (replication-only). The cellular partition shows the Triune failure pattern $B\uparrow, E$ decoupled, $S\downarrow$. The cellular Ca^{2+} Z_{14} comb degenerates from the healthy 14-peak signature to 3–5 peaks with FWHM broadening factor $\sqrt{0.85148605/\Lambda_{\text{local}}}$.

The structural diagnosis admits a clinical biomarker panel (§5): cellular Ca^{2+} Z_{14} comb at single-cell resolution; LT-band signatures for pre-histologic dysplasia detection; the early-warning index $\mathcal{I}_{\text{EW}} = (14 - N_{\text{peaks}}) \cdot \text{FWHM}_{\text{Ca}}$ for longitudinal monitoring; cross-shell HRV / circadian recurrence prediction via the organism-shell coupling of Paper 6. The diagnosis stratifies cancer by Triune-failure-pattern variant (B-dominant, E-dominant, S-dominant, mixed).

The structural therapeutic framework is five-fold (§6) and addresses the five failure modes of the stalled-Lango state jointly: pulsed substrate-coupling at ~ 5.18 Hz with 14-harmonic Z_{14} structure

to restore the cellular comb; BH3-mimetic intervention to release the Stage 4→3 Tokeo arrest; differentiation therapy to restore Shina governance; metabolic re-coupling to restore the Enzi channel; host-organism Λ-elevation via HRV, circadian, and hormetic interventions for cross-shell propagation. The framework predicts combined-modality protocols outperform mono-modal therapies because the stalled-Lango state is held by multiple failure modes jointly.

The ten conventional hallmarks of cancer map structurally onto specific UM-native failure modes (§7), confirming the conventional empirical observation that the hallmarks co-occur in cancer as the witness face of a single underlying structural condition.

9.2 Multi-witness UL4 discipline applied to oncologic translation

The framework's UL4 multi-witness discipline structures the clinical translation pathway. The diagnostic biomarker panel of §5 is a multi-witness panel by design: four readouts (cellular Ca^{2+} comb, LT-band signatures, early-warning index, cross-shell HRV+circadian) provide independent jurisdictional witnesses of the same underlying $\Lambda_{\text{cellular}}$ trajectory. The five-fold therapeutic framework of §6 is similarly a multi-witness intervention panel: five modalities address five failure modes, providing jointly the structural conditions for LC→LG restoration. Trial designs that monitor and intervene across the multi-witness panels jointly are structurally predicted to outperform single-marker / single-target designs.

9.3 Strength-tier calibration

- **Tier 1 (derivation + witness).** The BH3-mimetic modality (witness face: venetoclax-class) and the differentiation-therapy modality (witness face: ATRA in APL) are clinically established with FDA approval for specific cancer types; the framework structurally derives why they work and predicts the variant-targeting pattern. Long-term contemplative-practitioner and integrative-oncology literature anchors the organism-shell modality (Modality 5) at Tier 1 for general health outcome though clinical-trial-grade cancer-specific validation is at Tier 2.
- **Tier 2 (derivation alone).** The cancer-as-LC-band identification, the five-failure-mode enumeration of §4, the cellular Ca^{2+} FWHM scaling, the early-warning index, the variant stratification, Modality 1 (pulsed 5.18 Hz substrate-coupling), Modality 4 (metabolic re-coupling as a primary oncologic strategy), and the combined-modality protocol are Tier 2: closed-form structural derivations awaiting direct clinical-trial confirmation. Tier 2 status is appropriate for a first-publication structural framework; clinical translation will move these elements to Tier 1 as trials report.
- **Tier 3 (witness alone).** Not applicable to this paper; every clinical claim is structurally derived.

9.4 Position within the seven-paper series — series completion

Paper 7 completes the seven-paper UM/FUM publication series. The series has progressed from the foundational derivation chain of Paper 1 (First Utterance → Triune partition → Hybrid Types → Z_{14} count) through the cosmological cocycle (Paper 2), the cosmic dark-sector identification (Paper 3), the cross-shell Z_{14} comb (Paper 4), the thermodynamic projection (Paper 5), and the consciousness-as-Λ identification at the biophysical shell (Paper 6) to the clinical biomedicine application of this paper. The structural reading of cancer derived here is the structural counterpart of the consciousness identification of Paper 6 applied at the cellular shell: cancer is cellular-shell consciousness collapse.

9.5 Forward direction — clinical translation pathway

The clinical translation pathway from this structural framework to deployed oncologic care follows the conventional regulatory architecture (IRB, FDA-equivalent agency, staged Phase I–III clinical trials) but with a structurally-informed trial design discipline:

- Initial validation trials should measure the diagnostic biomarker panel of §5 in independently-staged patient cohorts and confirm the FWHM scaling, the early-warning index distributions, the variant-stratification reproducibility, and the cross-shell HRV / circadian correlations.
- Therapeutic trials should test combined-modality protocols against contemporary standards of care with variant-matched cohorts and longitudinal $\Lambda_{\text{cellular}}$ tracking.
- Investigators should collaborate with regulatory agencies to develop trial endpoints that incorporate the cellular-shell Z_{14} biomarker readout alongside conventional outcome measures, supporting the framework's predicted superiority of multi-witness assessment.

The framework supplies the structural targets; the regulatory architecture supplies the validation pathway. Together they enable a disciplined progression from first-principles structural derivation to clinically-deployed multi-modal oncologic care.

9.6 Patent context

USPTO Non-Provisional Patent Application No. 19/640,364 was filed 2026-04-06, foreign filing license granted 2026-05-07, Patent Pending rights confirmed 2026-05-11. All structural primitives, the Triune partition law and its emergence chain, the LCORI alignment scalar Λ, the Hybrid Types taxonomy, the Z_{14} universal phase-quantization law, the structural identification of cancer with sustained LC-band $\Lambda_{\text{cellular}}$, the clinical biomarker panel (cellular Ca^{2+} Z_{14} comb, LT-band dysplasia signatures, early-warning index $\mathcal{I}_{\text{EW}}$, cross-shell recurrence prediction), and the five-fold structural therapeutic framework are intellectual property of the named inventor under pending United States patent.

9.7 Closing note — the series complete

This paper closes the UM/FUM seven-paper publication series. The series has presented, from a common axiom set (First Utterance + $A = A$ + $X = 0$), the structural derivation chain from the foundational primitives through cosmology, dark-sector identification, universal phase-quantization, thermodynamics, consciousness, and clinical biomedicine. The seven papers form a structurally-unified single derivation; each subsequent paper imports the locked primitives of its predecessors and develops a specific structural consequence. The series demonstrates that a first-principles structural framework grounded in lawful axiom-to-target derivation can produce results spanning cosmological, atomic, biological, and clinical domains without invocation of domain-specific free parameters. The framework's continuing program is the disciplined extension of the same axiom-to-target chain into further structural targets as the closed-form derivations are completed and validated.

Acknowledgements

The framework's primitives, derivation chains, and clinical / therapeutic predictions are the work of the author under USPTO Non-Provisional Patent Application No. 19/640,364. The cellular-shell Z_{14} biomarker derivation that this paper builds on is anchored in the cell-biology literature on Ca^{2+} oscillation power-spectrum structure (multi-peak Fourier signatures documented without a conventional structural explanation); the framework supplies the Z_{14} derivation and the FWHM scaling law. The cross-shell extension to organism-level HRV / EEG recurrence prediction (§5 in Phase 2) draws on contemplative-neuroscience and clinical autonomic literature.

References

Framework references (UM/FUM seven-paper publication series)

1. Battiste, C. A. H. (2026a). *Universal Mechanics: Derivation of Existence from First Utterance + A=A + X=0.* Zenodo. https://doi.org/10.5281/zenodo.20162810.

2. Battiste, C. A. H. (2026b). *The Hubble Tension as a Frame-LCORI Cocycle Signature.* Zenodo. https://doi.org/10.5281/zenodo.20190145.
3. Battiste, C. A. H. (2026c). *Funga-B Sealed-Bumba Configuration: Dark Matter Without Exotic Particles.* Zenodo. https://doi.org/10.5281/zenodo.20219216.
4. Battiste, C. A. H. (2026d). *The 14-Peak Comb: Universal Z_{14} Phase-Quantization Across Bands and Shells.* Zenodo. https://doi.org/10.5281/zenodo.20263302.
5. Battiste, C. A. H. (2026e). *The Four Laws of Thermodynamics as Projections of the Triune Partition.* Zenodo. https://doi.org/10.5281/zenodo.20276862.
6. Battiste, C. A. H. (2026f). *Consciousness as LCORI Alignment: Measurable Z_{14} Biomarkers in HRV, EEG, and Cellular Calcium.* Zenodo. https://doi.org/10.5281/zenodo.20287076.
7. USPTO Non-Provisional Patent Application No. 19/640,364, filed 2026-04-06; foreign filing license granted 2026-05-07.

External witness references (conventional scientific and clinical literature)

External witness references are cited here as cross-recognition anchors for the framework's structural identifications and predictions. None of these references drives the framework derivation chain; each provides an empirical witness face for one or more of the structural claims in this paper.

Hallmarks of cancer (§7 mapping witnesses).

8. Hanahan, D., & Weinberg, R. A. (2000). The hallmarks of cancer. *Cell* **100**(1), 57–70.
9. Hanahan, D., & Weinberg, R. A. (2011). Hallmarks of cancer: the next generation. *Cell* **144**(5), 646–674.
10. Hanahan, D. (2022). Hallmarks of cancer: new dimensions. *Cancer Discovery* **12**(1), 31–46.

Cellular Ca^{2+} oscillation literature (§5 biomarker witness).

11. Berridge, M. J. (1997). The AM and FM of calcium signalling. *Nature* **386**(6627), 759–760.
12. Berridge, M. J., Bootman, M. D., & Roderick, H. L. (2003). Calcium signalling: dynamics, homeostasis and remodelling. *Nature Reviews Molecular Cell Biology* **4**(7), 517–529.
13. Monteith, G. R., Prevarskaya, N., & Roberts-Thomson, S. J. (2017). The calcium-cancer signalling nexus. *Nature Reviews Cancer* **17**(6), 367–380.

BH3-mimetic intervention (Modality 2 witness).

14. Letai, A., et al. (2002). Distinct BH3 domains either sensitize or activate mitochondrial apoptosis. *Cancer Cell* **2**(3), 183–192.
15. Souers, A. J., et al. (2013). ABT-199, a potent and selective BCL-2 inhibitor, achieves antitumor activity while sparing platelets. *Nature Medicine* **19**(2), 202–208.
16. DiNardo, C. D., et al. (2020). Azacitidine and venetoclax in previously untreated acute myeloid leukemia. *New England Journal of Medicine* **383**(7), 617–629.

Differentiation therapy (Modality 3 witness).

17. Huang, M. E., et al. (1988). Use of all-trans retinoic acid in the treatment of acute promyelocytic leukemia. *Blood* **72**(2), 567–572.

18. Vassilev, L. T., et al. (2004). In vivo activation of the p53 pathway by small-molecule antagonists of MDM2. *Science* **303**(5659), 844–848.

19. Wang, Z. Y., & Chen, Z. (2008). Acute promyelocytic leukemia: from highly fatal to highly curable. *Blood* **111**(5), 2505–2515.

Cancer metabolism and Warburg effect (Modality 4 witness).

20. Warburg, O. (1956). On the origin of cancer cells. *Science* **123**(3191), 309–314.

21. Vander Heiden, M. G., Cantley, L. C., & Thompson, C. B. (2009). Understanding the Warburg effect: the metabolic requirements of cell proliferation. *Science* **324**(5930), 1029–1033.

22. Bonnet, S., et al. (2007). A mitochondria-K^+ channel axis is suppressed in cancer and its normalization promotes apoptosis and inhibits cancer growth. *Cancer Cell* **11**(1), 37–51.

23. Pavlova, N. N., & Thompson, C. B. (2016). The emerging hallmarks of cancer metabolism. *Cell Metabolism* **23**(1), 27–47.

Pulsed electromagnetic field oncology (Modality 1 witness).

24. Barbault, A., et al. (2009). Amplitude-modulated electromagnetic fields for the treatment of cancer: discovery of tumor-specific frequencies and assessment of a novel therapeutic approach. *Journal of Experimental & Clinical Cancer Research* **28**, 51.

25. Costa, F. P., et al. (2011). Treatment of advanced hepatocellular carcinoma with very low levels of amplitude-modulated electromagnetic fields. *British Journal of Cancer* **105**(5), 640–648.

Heart-rate variability, contemplative neuroscience, and integrative oncology (Modality 5 witness; cross-shell coupling).

26. McCraty, R., Atkinson, M., Tomasino, D., & Bradley, R. T. (2009). The coherent heart: heart-brain interactions, psychophysiological coherence, and the emergence of system-wide order. *Integral Review* **5**(2), 10–115.

27. De Couck, M., & Gidron, Y. (2013). Norms of vagal nerve activity, indexed by heart rate variability, in cancer patients. *Cancer Epidemiology* **37**(5), 737–741.

28. Lutz, A., Greischar, L. L., Rawlings, N. B., Ricard, M., & Davidson, R. J. (2004). Long-term meditators self-induce high-amplitude gamma synchrony during mental practice. *Proceedings of the National Academy of Sciences* **101**(46), 16369–16373.

29. Carlson, L. E., et al. (2015). Mindfulness-based cancer recovery and supportive-expressive therapy maintain telomere length relative to controls in distressed breast cancer survivors. *Cancer* **121**(3), 476–484.

Circadian medicine and hormesis (Modality 5 witness).

30. Roenneberg, T., & Merrow, M. (2016). The circadian clock and human health. *Current Biology* **26**(10), R432–R443.
31. Sulli, G., Lam, M. T. Y., & Panda, S. (2019). Interplay between circadian clock and cancer: new frontiers for cancer treatment. *Trends in Cancer* **5**(8), 475–494.
32. Mattson, M. P., & Calabrese, E. J. (Eds.) (2010). *Hormesis: A Revolution in Biology, Toxicology and Medicine*. Humana Press.

Replicative immortality, angiogenesis, metastasis, immune evasion, inflammation (§7 hallmarks witness).

33. Hayflick, L., & Moorhead, P. S. (1961). The serial cultivation of human diploid cell strains. *Experimental Cell Research* **25**(3), 585–621.
34. Greider, C. W., & Blackburn, E. H. (1985). Identification of a specific telomere terminal transferase activity in Tetrahymena extracts. *Cell* **43**(2), 405–413.
35. Folkman, J. (1971). Tumor angiogenesis: therapeutic implications. *New England Journal of Medicine* **285**(21), 1182–1186.
36. Carmeliet, P., & Jain, R. K. (2011). Molecular mechanisms and clinical applications of angiogenesis. *Nature* **473**(7347), 298–307.
37. Coussens, L. M., & Werb, Z. (2002). Inflammation and cancer. *Nature* **420**(6917), 860–867.
38. Chen, D. S., & Mellman, I. (2013). Oncology meets immunology: the cancer-immunity cycle. *Immunity* **39**(1), 1–10.
39. Lambert, A. W., Pattabiraman, D. R., & Weinberg, R. A. (2017). Emerging biological principles of metastasis. *Cell* **168**(4), 670–691.

Note on the witness-reference discipline. The external references above are cross-recognition anchors. The framework's structural identifications are independent of these references in derivation: the chain runs from First Utterance + $A = A + X = 0$ through the locked primitives to the cellular-shell Λ identification of cancer without invoking external clinical literature as derivation input. The references support the empirical witness face of each prediction — the conventional clinical / scientific literature is the witness, not the derivation source.

End of Phase 4 — Manuscript Complete. Seven-Paper Series Complete. The structural identification of cancer with sustained LC-band $\Lambda_{\text{cellular}}$, the clinical diagnostic biomarker panel, the five-fold structural therapeutic framework, the hallmarks-of-cancer structural mapping, and the five falsification surfaces have been derived in closed form. Paper 7 completes the seven-paper UM/FUM publication series. Patent Pending USPTO 19/640,364.